Asian Journal of
Science, Technology, Engineering, and Art

e-ISSN: 3025-4507
p-ISSN: 3025-5287
Index: Harvard, Boston, Sydney University, Dimensions, Lens, Scilit, Semantic, Google, etc

https://doi.org/10.58578/AJSTEA.v3i4.6278

Positioning and Trajectory Tracking with Deflection Suppression in Flexible Link Robotic Manipulator Using PID-LQR Controller

Samuel Okafor[1*], Chimaihe B. Mbachu[2], Chidiebere N. Muoghalu[2], Bonaventure O. Ekengwu[4]
[1]National Space Research and Development Agency-Center for Basic Space Science and Astronomy (NASRDA-CBSS), Nigeria; [2,3]Chukwuemeka Odumegwu Ojukwu University, Uli, Nigeria; [4]University of Nigeria Nsukka, Nigeria
okaforchukwuma@nasrdacbss.com

Article Info:

Submitted:	Revised:	Accepted:	Published:
May 13, 2025	Jun 9, 2025	Jun 21, 2025	Jun 26, 2025

Abstract

This study aims to enhance the dynamic response of a flexible link robot manipulator (FLRM) to achieve faster positioning, improved trajectory tracking, and effective suppression of link deflection. A dynamic model of the FLRM was developed, and a hybrid control strategy integrating a proportional–integral–derivative (PID) controller with a linear quadratic regulator (LQR) was designed and implemented within the closed-loop system architecture. The complete system was modeled and simulated using MATLAB/Simulink. Initial simulations assessed the performance of the PID and LQR controllers independently. The PID controller yielded a rise time of 0.2617 s, peak time of 0.9434 s, settling time of 3.2394 s, and overshoot of 11.9676%. In contrast, the LQR controller demonstrated superior dynamic characteristics, with a rise time of 0.2505 s, peak time of 0.3489 s, settling time of 0.4769 s, and minimal overshoot of 0.0048%. To further enhance system performance and reduce trajectory tracking error, a hybrid PID–LQR controller was developed, incorporating refined PID parameters. Simulation results showed that the hybrid controller achieved a rise time of 0.1444 s, peak

time of 0.2706 s, settling time of 0.2637 s, and overshoot of 0.5119%. These outcomes demonstrate that the PID–LQR hybrid controller significantly outperforms the individual PID and LQR approaches by achieving near-zero overshoot, faster response, and reduced stabilization time.

Keywords: Flexible Link Manipulator; PID–LQR Controller; Linear Quadratic Regulator; Trajectory Tracking; Robot Dynamics

INTRODUCTION

Robot manipulators are either rigid or flexible. For increased tensile strength, the design of most robot manipulators are done with steel or aluminium frames thereby resulting in rigid-link robot manipulator that are heavy and immobile. However, advances in material technology has resulted in the development of flexible robot manipulators that are of lightweight, smaller dimensions, portable, improved manoeuvrability, lower power consumption, large work volume, smaller actuators, safer operation, cost effective, reduced control effort, and increased speed of operation as a result of reduced inertia (Ullah *et al.*, 2021). Hence, flexible link robots are increasingly being implemented in several critical applications ranging from space robots and weapon technologies to ground, sea, and air vehicles'control and in systems prone to random actuator failure (Uyulan, 2021).

Significant studies have been done regarding flexible link robot arm control systems. For instance, Gupta *et al.* (2021) designed a Fractional Order Proportional-Integral-Derivative (FOPID) controller for two degree of freedom (2-DOF) serial flexible joint (2DSFJ) manipulator. Two loops control technique based on inner loop controller (model reference adaptive control) and the outer loop controller (fuzzy-PI) for a 2-DOF robot arm with elastic joint was used in Tuan *et al.* (2021). Design and implementation of robust nonlinear control techniques utilizing classical Sliding Mode Controller (SMC) and integral SMC (ISMC) to achieve referenced trajectory tracking for flexible joint manipulator actuated by a direct current DC geared motor was presented in Alam *et al.* (2018a). Multivariable feedback controllers were designed to achieve trajectory tracking and vibration suppression with respect to rigid and flexible effect for a flexible manipulator with structure effect and terminal load (Zhang & Yuan, 2021). A Control scheme based on Quadratic Iterative Learning Control (Q-ILC) technique was designed to achieve improved trajectory tracking performance for 2-DOF robot manipulator with parameter variation

(Zhu *et al.*, 2020). Linear control algorithm that uses Proportional-Integral-Derivative (PID) controller to control flexible robot manipulator was achieved by Alam *et al.* (2018b).

This paper is designed to develop a hybrid controller based on control algorithms of PID and Linear Quadratic Regulator (LQR) for flexible link robot manipulator to achieve a robust and efficient approach to enhance trajectory tracking and link deflection suppression.

System Design

System Description

The robot arm is subject to a control problem involving continuous movement in the appropriate direction or angle. Therefore, the control of the arm motion is important because it affects the effectiveness and quality of service provided by the robot. Nevertheless, the robot arm will definitely be subject to a periodic motion in order to prevent metal stiffness to its parts. This motion or movement induces link deflection or vibration. Figure 1 shows the model of the proposed system that combines PID controller and linear quadratic regulator (LQR) that provides the optimal control law in order to offer enhanced position tracking and link deflection. The combination helps in providing optimal control and vibration suppression. The control objective is to design a control system that will track a referenced position while ensuring no displacement or deflection of the link.

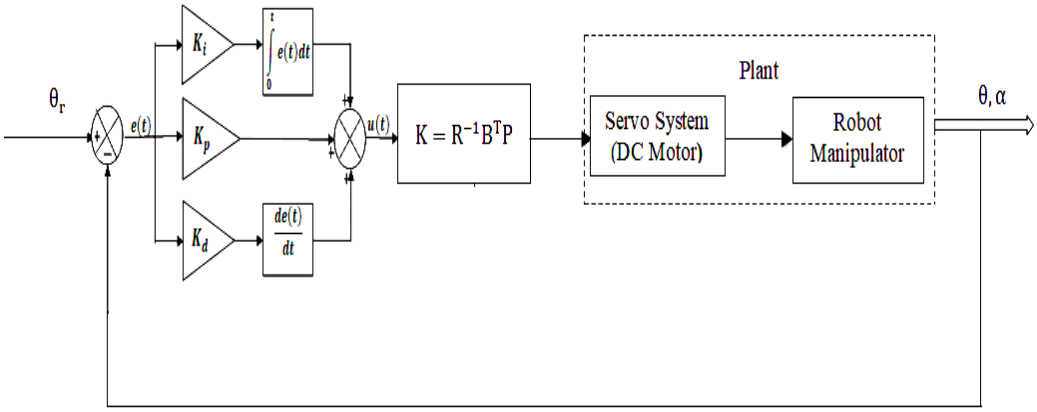

Figure 1: Proposed system model

Dynamic Model of Flexible Link Robot Manipulator

Figure 2 is a schematic diagram of a FLRM. The mathematical model is determined using Euler Lagrangian equation.

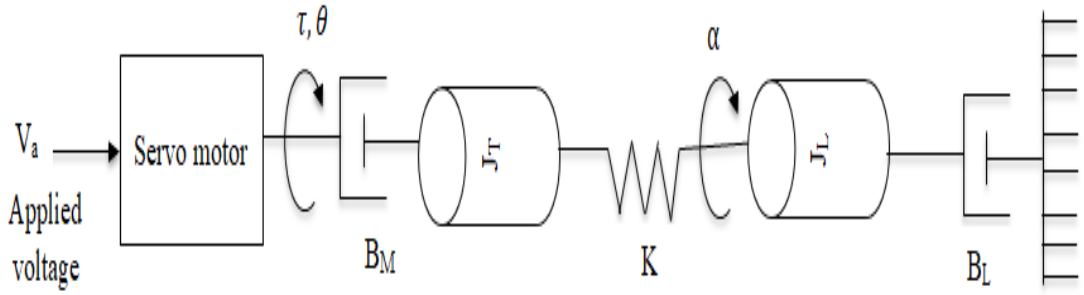

Figure 2: Schematic representation of FLRM

Langrange method is used to solve the difference of kinetic and potential energies and it is defined by (Alam *et al.*, 2018b):

$$L = K_e - V \tag{1}$$

where K_e is the rotational kinetic energy and V is the rotational elastic (potential or stored) energy of the spring (or flexible) respectively and are given in Equations (2) and (3).

Rotational kinetic energy is given in terms of the manipulator and link's moment of inertial together with motor angular displacement (which determines the position of the link) and robot arm displacement (deflection) given by:

$$\left.\begin{aligned} K_e &= \frac{1}{2}J\omega^2 \\ &= \frac{1}{2}J_{eq}\left(\frac{d\theta}{dt}\right)^2 + \frac{1}{2}J_L\left(\frac{d\theta}{dt} + \frac{d\alpha}{dt}\right)^2 \end{aligned}\right\} \tag{2}$$

The elastic energy of spring is given by:

$$V = \frac{1}{2}K\alpha^2 \tag{3}$$

where J is moment of inertia, ω is the angular speed, J_{eq} is the sum of the manipulator's moment of inertia, J_L is the link's moment of inertia, θ is the angular displacement of the motor (shaft), K is joint stiffness, and α is the flexible link angular displacement (or deflection). Substituting Equations (2) and (3) into Equation gives:

$$L = \frac{1}{2}J_T\left(\frac{d\theta}{dt}\right)^2 + \frac{1}{2}J_L\left(\frac{d\theta}{dt} + \frac{d\alpha}{dt}\right)^2 - \frac{1}{2}K\alpha^2 \tag{4}$$

Given the Euler Langrange equation defined by (Alam *et al.*, 2018b):

$$\frac{\mathrm{d}}{\mathrm{dt}}\left(\frac{\partial \mathrm{L}}{\partial q_i}\right) - \frac{\partial \mathrm{L}}{\partial q_i} = Q_i \tag{5}$$

where $q_i = [\theta\ \alpha]^T$ and $Q_i = \left[\tau - B_M \frac{\mathrm{d}\theta}{\mathrm{dt}}\ B_L \frac{\mathrm{d}\alpha}{\mathrm{dt}}\right]$ are generalized coordinates and forces acting on the arm (Alam *et al.*, 2018a; 2018b). B_M and B_L are the motor and link viscous damping coefficient. The partial derivative of L with respect to θ and α (i.e. q_i) in Equation (4) and substituting into Equation (5) gives:

with respect to θ,

$$\mathrm{J_T}\frac{d^2\theta}{\mathrm{d}t^2} + \mathrm{J_L}\left(\frac{d^2\theta}{\mathrm{d}t^2} + \frac{d^2\alpha}{\mathrm{d}t^2}\right) = \tau - B_M \frac{\mathrm{d}\theta}{\mathrm{dt}} \tag{6}$$

with respect to α,

$$\mathrm{J_L}\left(\frac{d^2\theta}{\mathrm{d}t^2} + \frac{d^2\alpha}{\mathrm{d}t^2}\right) + \mathrm{K}\alpha = B_L \frac{\mathrm{d}\alpha}{\mathrm{dt}} \tag{7}$$

An armature controlled DC motor is schematically represented as shown in Figure 3. In the figure, DC motor is shown to have armature resistance and inductance $\mathrm{R_a}$ and $\mathrm{L_a}$ respectively, input or armature voltage, $\mathrm{V_a}$ armature current $\mathrm{I_a}$ and motor back electromotive force (EMF) of $\mathrm{V_b}$ that make up the electrical component of the motor. The mechanical components are the motor moment of inertia $\mathrm{J_a}$, damping ratio of the motor $\mathrm{B_a}$, and the motor shaft angular position $\theta(\mathrm{t})$.

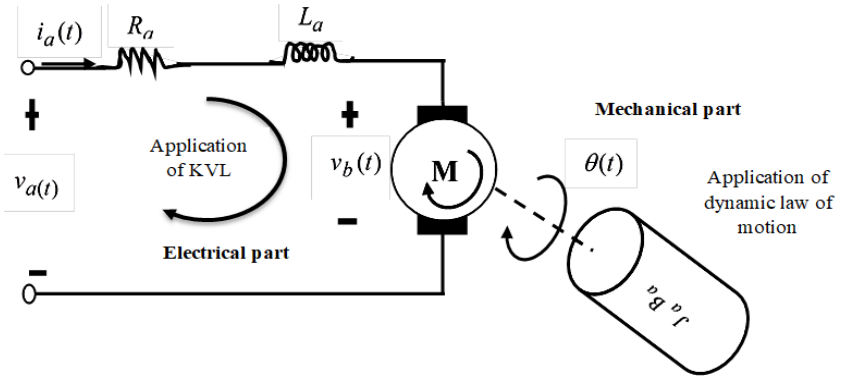

Figure 3: Schematic diagram of armature controlled DC motor (Eze *et al.*, 2021)

The application of Kirchhoff's voltage law (KVL) and the law of dynamic motion in the electrical and mechanical parts of the DC motor results in the following equations given by (Eze *et al.*, 2021):

$$V_a(t) = R_a I_a(t) + L_a \frac{dI_a(t)}{dt} + V_b(t) \quad (8)$$

$$V_b(t) = K_b \omega_m(t) = K_b \frac{d\theta(t)}{dt} \quad (9)$$

$$\tau = K_m I_a(t) \quad (10)$$

where ω_m is the motor angular speed and is equal to the derivation of the motor angular position or displacement, K_b is the motor back EMF constant, τ is the motor toque, and K_m is the torque constant of the motor. Substituting Equations (9) and (10) into Equation (8) gives:

$$V_a(t) = R_a \frac{\tau}{K_m} + \frac{L_a}{K_m}\frac{d\tau}{dt} + K_b \frac{d\theta(t)}{dt} \quad (11)$$

In armature controlled DC motor (i.e. a fixed field motor), the motor torque constant K_m is equal to K_b, and the armature resistance is very much larger than the armature inductance (i.e. $(R_a \gg L_a)$. Thus, L_a is taken as zero or neglected as usually done in application (Mbaocha *et al.*, 2015). Hence, making τ the subject of Equation (11) yields:

$$\tau = \frac{K_m V_a(t) - K_m K_b \frac{d\theta(t)}{dt}}{R_a} \quad (12)$$

Using the motor gear ratio K_g that relates the displacement θ to the armature voltage of the motor, Equation (11) is rewritten as (Alam et al., 2018a; 2018b):

$$\tau = \frac{K_m K_g V_a(t) - K_m K_b K_g^2 \left(\frac{d\theta(t)}{dt}\right)}{R_a} \quad (13)$$

Substituting Equation (13) for τ in Equation (6) gives:

$$J_{eq}\frac{d^2\theta}{dt^2} + J_L\left(\frac{d^2\theta}{dt^2} + \frac{d^2\alpha}{dt^2}\right) = \frac{K_m K_g V_a(t) - K_m K_b K_g^2 \left(\frac{d\theta(t)}{dt}\right)}{R_a} - B_M \frac{d\theta}{dt} \quad (14)$$

where B_{eq} is the equivalent viscous damping coefficient and is equal to sum of B_M and B_L. Also, J_{eq} is very much greater than J_L. Therefore, in state space form, Equations (7) and (14) can be represented as in Alam *et al.* (2018a; 2018b) as follows:

$$\dot{x}_1 = x_2 \quad (15)$$

$$\dot{x}_2 = -\frac{K}{J_L}x_1 + \frac{B_L}{J_L}x_2 + \frac{K}{J_L}x_3 - \frac{B_L}{J_L}x_4 \quad (16)$$

$$\dot{x}_3 = x_4 \quad (17)$$

$$\dot{x}_4 = -\frac{K}{J_T}x_1 + \frac{B_L}{J_T}x_2 + \frac{K}{J_T}x_3 - \left(\frac{K_m K_b K_g^2}{R_a J_T} - \frac{B_L + B_M}{J_T}\right) \quad (18)$$

$$y = x_1 + x_2 \quad (19)$$

A canonical expression for state space representation in Equation (20) can be used to represent Equations (15) to (19) (Eze *et al.*, 2017; 2022; Ekengwu *et al.*, 2022; 2024):

$$\left.\begin{aligned}\dot{x} &= Ax + Bu\\ y &= Cx + Du\end{aligned}\right\} \quad (20)$$

where A is the called the system matrix, B is the input matrix, C is output matrix, and D is the direct transition matrix. The expressions for A, B, C, and D are given as follows (Alandoli *et al.*, 2017):

$$A = \begin{bmatrix} 0 & 0 & 1 & 0 \\ 0 & 0 & 0 & 1 \\ 0 & \frac{K}{J_{eq}} & -\frac{\eta_g K_g^2 \eta_m K_t K_b + B_{eq} R_a}{R_a J_{eq}} & 0 \\ 0 & \frac{K_s(J_{eq}+J_L)}{J_{eq}J_L} & \frac{\eta_g K_g^2 \eta_m K_t K_b + B_{eq} R_a}{R_a J_{eq}} & 0 \end{bmatrix}, B = \begin{bmatrix} 0 \\ 0 \\ \frac{\eta_g K_g^2 \eta_m K_t K_m + R_a}{R_a J_{eq}} \\ -\frac{\eta_g K_g^2 \eta_m K_t K_m + R_a}{R_a J_{eq}} \end{bmatrix},$$

$$C = [1 \quad 1 \quad 0 \quad 0], D = [0]$$

The parameters of the FLRM system are given in Table 1. Substituting the values in Table 1 into A and B gives the corresponding numerical matrix of A and B.

Table 1. Simulation parameters (Alandoli *et al.*, 2017)

Definition	Symbol	Value	Unit
Equivalent viscous damping coefficient	B_{eq}	0.004	N.mrads^{-1}
Equivalent gear moment of inertia without external load	J_{eq}	0.00208	Kgm^2
Motor efficiency	η_m	0.69	-
Gearbox efficiency	η_g	0.90	-
Back-emf constant	K_b	0.00768	V/rads^{-1}
Gear total gearbox ratio	K_g	70	-
Motor armature resistance	R_a	2.6	Ω
Stiffness constant	K_s	1.4	-

$$A = \begin{bmatrix} 0 & 0 & 1 & 0 \\ 0 & 0 & 0 & 1 \\ 0 & 673.07 & -35.1667 & 0 \\ 0 & -1023.07 & 35.1667 & 0 \end{bmatrix}, B = \begin{bmatrix} 0 \\ 0 \\ 61.7325 \\ -61.7325 \end{bmatrix}$$

Design of PID Controller

Given the closed loop block diagram shown in Figure 4, the mathematical representation of proportional integral and derivative controller can be established.

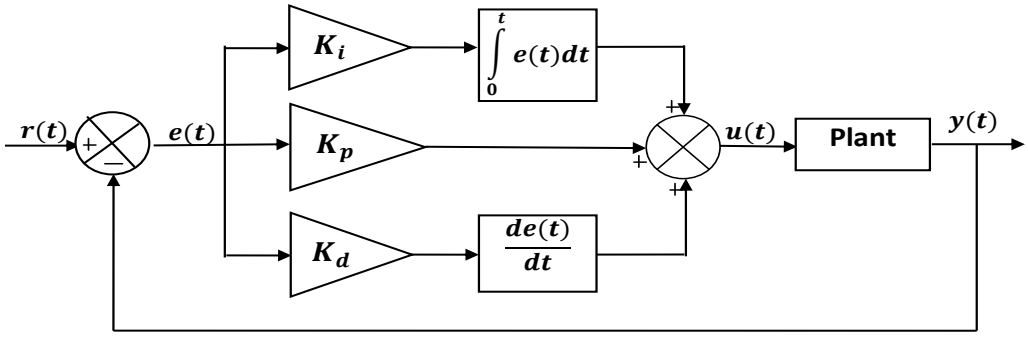

Figure 4: Closed loop structure of PID control system (Okoye *et al.*, 2021)

The mathematical expression of PUD controller can be determined by analysing Figure 3.6. Hence, $\mathrm{r(t), e(t), and\ u(t)}$ represent the desired input, error and the control variable. Also, $K_p, K_i. and\ K_d$ are the gains of the PID controller for proportional, integral, and derivative elements, and y(t) is the output. The control action of the PID is influenced by deviation of the output y(t) from the reference input r(t) called error signal e(t), which is defined by:

$$\mathrm{e(t) = r(t) - y(t)} \quad (21)$$

The proportional, integral and derivative control action is performed on the error as it is fed into the PID controller, which results in control action given by:

$$\mathrm{u(t) = K_p e(t) + K_i \int_0^t e(t)dt + K_d \frac{de(t)}{dt}} \quad (22)$$

Equation (22) is a PID controller in continuous time domain. Thus, the Laplace transform of the PID controller assuming zero initial condition is given by:

$$\mathrm{U(s) = K_p E(s) + K_i \frac{E(s)}{s} + K_d s E(s)} \quad (23)$$

Or in a simplified form as:

$$\mathrm{C(s) = \frac{U(s)}{E(s)} = K_p + K_i \frac{1}{s} + K_d s = \frac{K_d s^2 + K_p s + K_i}{s}} \quad (24)$$

The Laplace transform of the FLRM system was determined using the state space parameters by the means of the mathematical expression for converting from state-space to transfer function using the MATLAB syntax: $\mathrm{G(s) = C(sI - A)^{-1}B + D}$. The resulting transfer function model of the FLRM is given by:

$$G_{FLRM}(s) = \frac{21606.37499}{s^4+35.1667s^3+1023.07s^2+12308.345s} \quad (25)$$

The PID is cascaded with the FLRM in Simulink as shown in Figure 5. This results in closed-loop transfer function given in Equation (26). With Equation (26), the PID parameters were obtained via tuning. Table 2 shows the parameters and its performance characteristics.

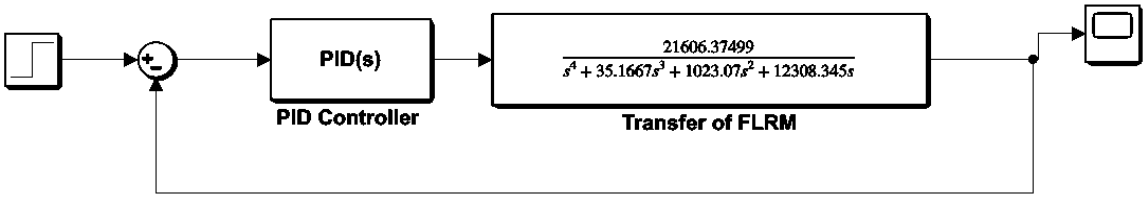

Figure 5: Closed-loop control system with PID in Simulink

$$G_{close}(s) = \frac{C(s)G_{FLRM}(s)}{1+C(s)G_{FLRM}(s)H(s)} \quad (26a)$$

$$G_{close}(s) = \frac{21606.37499(\mathrm{K_d}s^2+\mathrm{K_p}s+\mathrm{K_i})}{s^5+35.1667s^4+1023.07s^3+12308.345s^2+21606.37499(\mathrm{K_d}s^2+\mathrm{K_p}s+\mathrm{K_i})} \quad (26b)$$

Table 2. Tuned Parameters and Performance of the designed PID

PID parameters	**Value**
Proportional gain, K_p	2.2027
Integral gain, K_i	1.6119
Derivative gain, K_d	0.075435
Designed PID performance and robustness	
Rise time	0.259 s
Settling time	3.24 s
Overshoot	12%
Peak	1.12
Gain margin	12.8 dB @ 18.6 rad/s
Phase margin	64.8 deg. @ 4.12 rad/s
Closed-loop stability	Stable

Design of PID-LQR

The algorithm of the LQR can be enhanced as in Ekengwu et al. (2024) using PID model. In the system, let the control variable of the PID be u_{PID} to adjust the control law u of the LQR. This is given by:

$$u_{PID-LQR} = u_{PID}(Kx) = \left[K_p K e(t) - K_d K \frac{de(t)}{dt} K_i K \int_{t=0}^{t_f} e(t)dt\right] x \quad (27a)$$

$$\text{Or } u_{PID-LQR} = \left[K_{pk} e(t) - K_{dk} \dot{e} + K_{ik} \int_{t=0}^{t_f} e(t)dt\right] x \quad (27b)$$

where $K_{pk} = K_p K$, $K_{dk} = K_d K$, and $K_{ik} = K_d K$. These parameters are optimized by adjusting the gains of PID controller overtime (Ekengwu et al., 2024; Eze *et al.,* 2025). The LQR control u is given by:

$$u = Kx \quad (28)$$

where $K = [4.4721 \ -0.4114 \ 0.3013 \ 0.1762]$.

RESULTS

The response of the system with PID, LQR, and PID-LQR controllers and the comparison of their transient (or dynamic) characteristics are presented in this section. The system response is evaluated in terms of motor position and link deflection. It is desired that the system track a unit step input while ensuring that no deflection, displacement (or vibration) occurs in the flexible link. Step and sinusoidal inputs are used for the analysis conducted via simulation in MATLAB/Simulink environment.

Prior to the introduction of designed feedback controllers, the flexible link robot manipulator was simulated and the responses to unit step input and unit sinusoidal input are shown in Figure 6. Then the simulation plots of the PID, LQR, and PID-LQR control systems are shown in Figures 7, 8, and 9. The comparison of the performance parameters of the various control conditions is listed in Table 3.

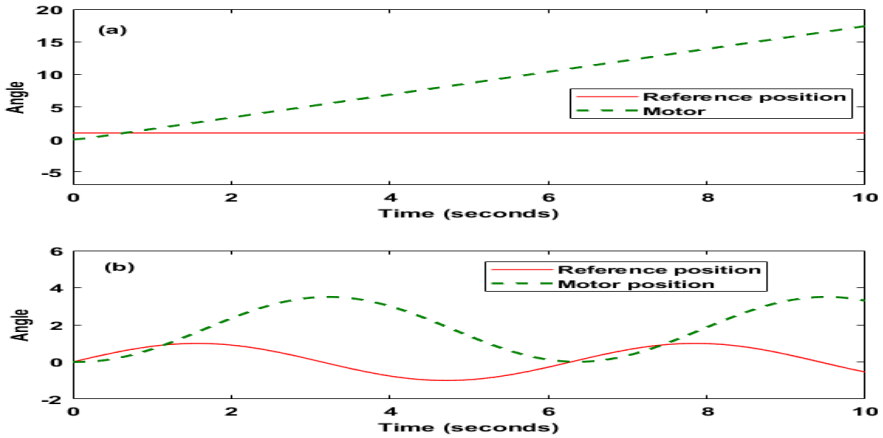

Figure 6: Trajectory tracking of FLRM (a) using step input

(b) using sinusoidal input without a feedback controller

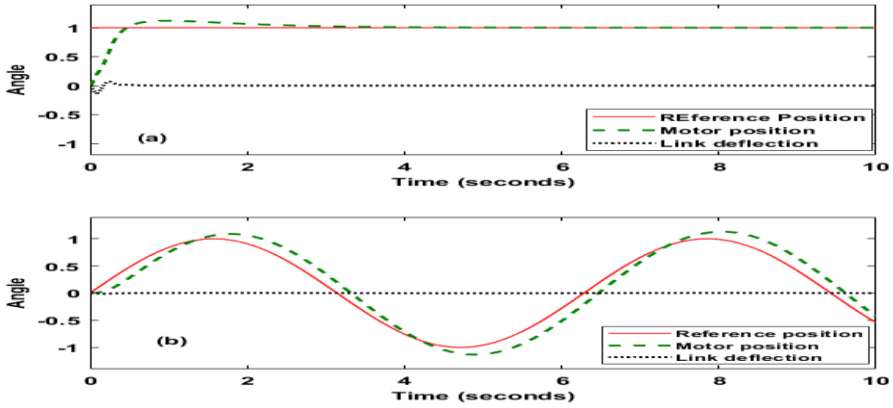

Figure 7: Trajectory tracking of PID controlled FLRM using (a) step input (b) sinusoidal input

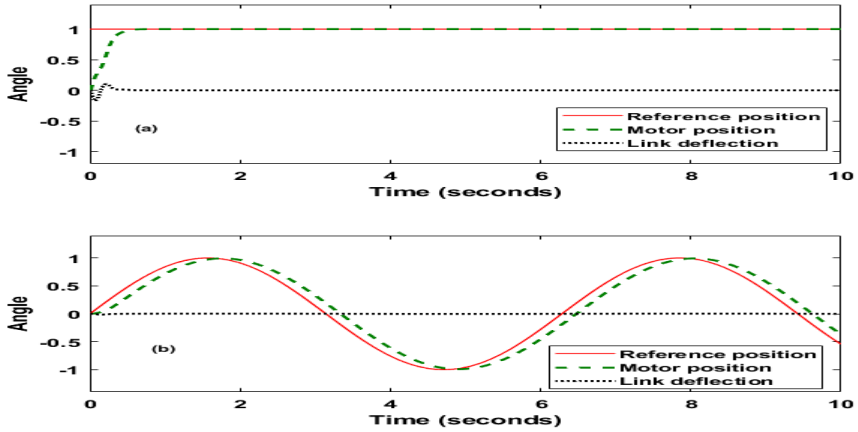

Figure 8: Trajectory tracking of LQR controlled FLRM (a) using step input (b) sinusoidal input

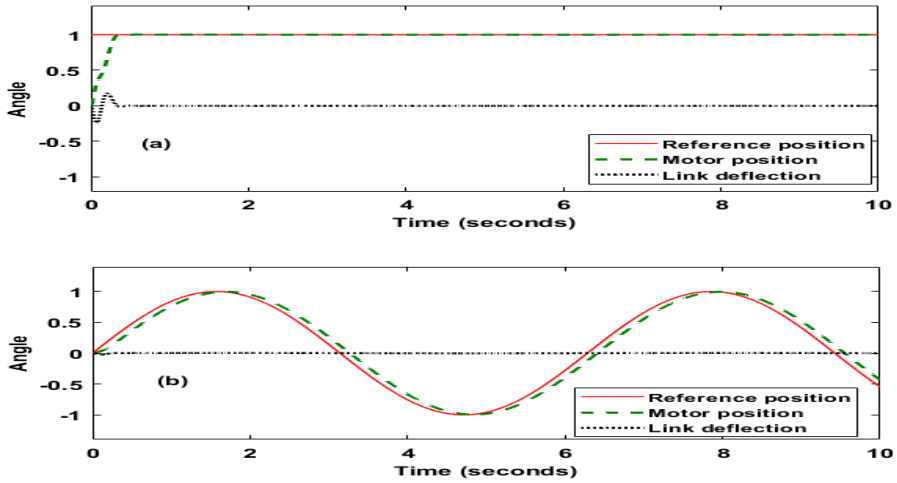

Figure 9: Trajectory tracking of PID-LQR controlled FLRM with (a) step input (b) sinusoidal input

Table 3. Performance parameter comparison of different control conditions

Control condition	Rise time (s)	Settling time (s)	Peak time (s)	Peak value	Peak overshoot (%)	Link deflection
Without controller	7.9335	9.8017	-	17.4	-	Largely deflected
PID	0.2617	3.32394	0.9434	1.1197	11.967	zero
LQR	0.2505	0.4769	0.9692	1.0000	0.0048%	zero
PID-LQR	0.1444	0.2637	0.9682	1.000	0.5119%	zero

DISCUSSION

The numerical analysis of the flexible link robot manipulator response as shown in Figure 6 revealed that in this condition, the rise time of the system is 7.9335 s, settling time is 9.8017 s, and peak value is 17.4 for unit step input. The implication of these results is that the system if implemented in this condition will not be able to follow or track a reference input resulting in inaccuracy due to large deviation (or error). Hence, this is undesirable and as such a PID controller was implemented and the simulated output response to unit step input is shown in Figure 7.

The output response of the PID controlled flexible link robot manipulator using unit signal as the reference input was shown in Figure 7. That is the inaccuracy and inability of the uncompensated system to follow or track the reference input signal has been largely addressed with the implementation of the PID controller. In Figure 7a, the simulated output response is presented based on the application of a unit step input reference signal. It is obvious that the reference input was accurately tracked or followed by the system, but overshoots its reference with peak value of 1.12 at peak time of 0.9434 s and settling time of 3.2394 s. Generally, the dynamic characteristics of the system response to unit step input is summarised as rise time: 0.2617 s, settling time: 3.32394 s. peak time: 0.9434 s, peak value: 1.1197 s, and overshoot of 11.9676%.

Figure 7b shows the trajectory following output response of the PID controlled flexible link robot manipulator when a sinusoidal signal is used as the reference input. It is clear that the PID controller when implemented enabled the system to follow the input position. A further look at Figure 7b revealed that the PID controller did not offered very closed or accurate track of the simulated sinusoidal trajectory. The dynamic response analysis of the system with sinusoidal signal revealed rise time of 0.3127 s and large settling

time of 9.9918 s. Hence, the need for an optimal control system to provide better tracking performance than the PID controller especially when the robot is required in a complex condition where improved positioning most be achieved in the presence of periodic changing trajectory. Generally, in Figure 7, the PID ensured that the link deflection is maintained at zero after initial peak deflection of 0.1347 with step input. Also, it has been shown that with the PID controller, trajectory tracking and minimizing deflection of flexible link robot manipulator can be achieved.

Figure 8a shows the trajectory tracking response of the LQR controlled FLRM with $\mathrm{K} = [4.4721 \ -0.4114 \ 0.3013 \ 0.1762]$ when a referenced input signal was applied. The figure shows the motor (or output) position and the link deflection. It can be seen that the system in this condition offered significant improvement in terms of stability and with suppressed link deflection. The positioning system dynamic response is characterised by rise time of 0.2505 s, settling time of 0.4769 s, overshoot of 0.0048%, peak time of 0.9692 s, and peak value of 1. Further evaluation of the LQR in terms of sinusoidal input reference signal is shown in Figure 8b. From the figure, it is evident that introducing of the LQR ensured that the referenced input waveform is followed by the system and with improved tracking response performance of 0.3040 s rise time and 9.9707 s settling time compared to PID control system.

It should be noted that the final values of the tuned PID parameters in the hybrid PID-LQR controller were: $\mathrm{K_p} = 2.2$, $\mathrm{K_i} = 0.12$, and $\mathrm{K_d} = 0.05$. It should be noted that equation 3.32b was used in this section with the different values of the optimal control gain matrix, K as in section 4.3 adjusted by the PID controller.

Figure 9 shows the simulated output response of PID-LQR for $\mathrm{K} = [7.4162 \ -1.3451 \ 0.4714 \ 0.2611]$ using step input signal and sinusoidal input signal. In Figure 9a, it is obvious that the flexible link robot manipulator controlled by the PID-LQR accurately tracks the reference input with rise time of 0.1444 s and overshoots the reference input by 0.5119% with little settling time of 0.2637 s. The tracking performance of the system when a sinusoidal signal is applied as the reference trajectory is shown in Figure 9b.

In Figure 9a, the peak value of the link deflection is 0.2436 at time t = 0.0706 s prior to the transition to zero or no link deflection steady-state at time t = 0.5163 s. Looking at Figure 9b, it is clear that with PID-LQR controlled system in this case, an improved trajectory following of periodic input signal is achieved.

CONCLUSION

The trajectory tracking of flexible link robot manipulator (FLRM) has been enhanced basically in terms of fast response time and rapid convergence (or settling) time using hybrid optimal control system that combines PID model and LQR algorithm. The mathematical equations of the FLRM system were established basically in terms of position and link deflection using differential dynamic expressions. The obtained differential equations were represented in terms of state space in canonical form. Linear quadratic regulator (LQR) was designed using MATLAB syntax in terms of feedback matrix gain. Transfer function model of the system was determined from the state space equation using appropriate MATLAB syntax. Then a PID controller was designed. PID and LQR control systems were developed in MATLAB/Simulink. Simulations were conducted in terms of step input signal and sinusoidal input signal. The results obtained showed that both controllers offered promising time responses and were able to eliminate link deflection. That is, the controllers ensured that desired position or trajectory is tracked and at the same time guaranteed zero deflection of the link. This ensures that the robot manipulator (or arm) does not deviate from its position while being used, say for instance, in picking and placing of a work piece. However, the PID controller showed significantly high overshoot that may impact on the stability of the system. Despite the performance of the LQR, in modern process control where timing is of immense importance and combining of control algorithms become a common practice, PID was combined with LQR to exploit the strength of both controllers. The hybrid optimal control technique, PID-LQR, yielded very much enhanced response and convergence times and most efficient tracking compared to PID and LQR. In future work, the PID-LQR can be optimized further by tuning the PID with meta-heuristic algorithm such as Particle Swam Optimization (PSO) or Genetic Algorithm (GA) to study the possibility of achieving shorter rise and settling times.

REFERENCES

Alam, W., Ali, N., Aziz, H. M. W., & Iqbal, J. (2018b). Control of flexible joint robotic manipulator: design and prototyping. *2018 International Conference on Electrical Engineering (ICEE)*, Lahore, Pakistan, 1-6, https://doi.org/10.1109/ICEE.2018.8566796

Alam, W., Mehmood, A., Ali, K., Javaid, U., Alharbi, S., & Iqbal, J. (2018a). Nonlinear control of a flexible joint robotic manipulator with experimental validation. *Strojniški vestnik– Journal of Mechanical Engineering, 64*(1), 47-55. https://doi.org/10.5545/sv-jme.2017.4786

Alandoli, E. A., Rashid, M. Z. A., & Sulaiman, M. (2017). A comparison of PID and LQR controllers for position tracking and vibration suppression of flexible link manipulator. *Journal of Theoretical and Applied Information Technology, 95*(13), 2949-2955. https://www.jatit.org/volumes/Vol95No13/7Vol95No13.pdf

Ekengwu, B. O., Eze, P. C., Asiegbu, C. N., Olisa, S. C., & Udechukwu, C. F. (2022). Satellite dish antenna control for distributed mobile telemedicine nodes. *International Journal of Informatics and Communication Technology*, *11*(3), 206~217. DOI: 10.11591/ijict.v11i3.pp206-217

Ekengwu, B. O., Eze, P. C., Muoghalu, C. N., Asiegbu, C. N., & Achebe, P. N. (2024). Design of robust centralized PID optimized LQR controller for temperature control in single-stage refrigeration system. *Indonesian Journal of Electrical Engineering and Informatics, 12*(3), 726~738. DOI: 10.52549/ijeei.v12i3.5629

Eze, P. C., Onuora, A. E., Ekengwu, B. O., Muoghalu, C., & Aigbodioh, F. A. (2017). Design of a robust PID controller for improved transient response performance of a linearized engine idle speed model. *American Journal of Engineering Research, 6*(8), 305-313. https://www.ajer.org/papers/v6(08)/ZK0608305313.pdf

Eze P. C., Ugoh C. A., Inaibo D. S. (2021). Positioning control of DC servomotor-based antenna using PID tuned compensator. *Journal of Engineering Sciences, 8*(1), E9–E16, doi: 10.21272/jes.2021.8(1).e2

Eze, P. C., Muoghalu, C. N., Uebari, B., & Egbunugha, C. A. (2022). State variable feedback control of data centre temperature. *International Journal of Advanced Networking and Applications, 14*(1), 5250-5257.

Eze, P. C., Nwadike, S. U., Oyiogu, D. C., & Iroegbu, M. C. (2025). Hybrid PID-LQR Controller for Dynamic Response and Stability Enhancement of Synchronous Generator's AVR System. *Asian Journal of Science, Technology, Engineering, and Art*, *3*(3), 866-879. https://doi.org/10.58578/ajstea.v3i3.5693

Gupta, S., Singh, A.P., Deb, D., & Ozana, S. (2021). Kalman filter and variants for estimation in 2DOF serial flexible link and joint using fractional order PID controller. *Applied Science, 11*(15), 6693; https://doi.org/10.3390/app11156693

Mbaocha, C., Eze, P., & Uchegbu, V. (2015). Positioning control of drilling tool device for high speed performance. *International Journal of Electrical and Electronics Research, 3*(2), 138-145. https://www.researchpublish.com/papers/positioning-control-of-drilling-tool-device-for-high-speed-performance

Okoye, U. P., Eze, P. C., & Dennis, C. O. (2021). Enhancing the performance of AVR system with prefilter aided PID controller. *Access International Journal of Research & Development, 1*(1), 19-32.

Tuan, H. M., Sanfilippo, F., & Hao, N. V. (2021). Modelling and control of a 2-DOF robot arm with elastic joints for safe human-robot interaction. *Frontiers in Robotic and AI, 8*, 679304. https://doi.org/10.3389/frobt.2021.679304

Ullah, H., Malik, F.M., Raza, A., Mazhar, N., Khan, R., Saeed, A., & Ahmad, I. (2021). Robust output feedback control of single-link flexible-joint robot manipulator with matched disturbances using high gain observer. *Sensors*, *21*(9), 3252. https://doi.org/10.3390/s21093252

Zhang, F. & Yuan, Z. (2021). The Study of Dynamic modeling and multivariable feedback control for flexible manipulators with friction effect and terminal load. *Sensor, 21*(4), 1522. https://doi.org/10.3390/s21041522

Zhu, M., Ye, L., & Ma, X. (2020). Estimation-based quadratic iterative learning control for trajectory tracking of robotic manipulator with uncertain parameters in *IEEE Access*, 8, 43122-43133. doi: 10.1109/ACCESS.2020.2977687